Developmental Cell, Vol. 1, 621–631, November, 2001, Copyright ©2001 by Cell Press

Phosphorylation of γ-Tubulin Regulates Microtubule Organization in Budding Yeast

Jacalyn Vogel,[1] Ben Drapkin,[1] Jamina Oomen,[1] Dale Beach,[2] Kerry Bloom,[2] and Michael Snyder[1,3]

[1] Department of Cellular, Molecular, and Developmental Biology
Yale University
New Haven, Connecticut 06520

[2] Department of Biology
University of North Carolina, Chapel Hill
Chapel Hill, North Carolina 27599

Summary

γ-Tubulin is essential for microtubule nucleation in yeast and other organisms; whether this protein is regulated in vivo has not been explored. We show that the budding yeast γ-tubulin (Tub4p) is phosphorylated in vivo. Hyperphosphorylated Tub4p isoforms are restricted to G1. A conserved tyrosine near the carboxy terminus (Tyr445) is required for phosphorylation in vivo. A point mutation, Tyr445 to Asp, causes cells to arrest prior to anaphase. The frequency of new microtubules appearing in the SPB region and the number of microtubules are increased in *tub4-Y445D* cells, suggesting this mutation promotes microtubule assembly. These data suggest that modification of γ-tubulin is important for controlling microtubule number, thereby influencing microtubule organization and function during the yeast cell cycle.

Introduction

Microtubules are essential for many cellular processes including chromosome segregation, vesicle trafficking, nuclear positioning, and establishment of cell shape and polarity (Kellogg et al., 1994). In order to carry out their specialized functions, microtubules are organized into complex arrays by the microtubule-organizing center (MTOC). One key component of MTOCs is γ-tubulin (Oakley and Oakley, 1989), a conserved microtubule nucleation factor in eukaryotes (Oakley et al., 1990; Horio et al., 1991; Stearns et al., 1991; Zheng et al., 1991; Moritz et al., 1995; Sobel and Snyder, 1995; Vogel et al., 1997). To date, studies involving γ-tubulin have focused on the molecules with which it interacts (Raff et al., 1993; Zheng et al., 1995; Knop et al., 1997; Murphy et al., 1998) and how γ-tubulin is physically associated with microtubules (Moritz et al., 2000; Wiese and Zheng, 2000; Keating and Borisy, 2000) and MTOCs (Knop and Schiebel, 1998; Oegema et al., 1999; Gunawardane et al., 2000; Zhang et al., 2000). Little is known regarding the regulation of γ-tubulin in vivo.

Saccharomyces cerevisiae is an excellent model organism for the study of γ-tubulin or MTOC regulation and function. Yeast is readily amenable to genetic analysis, has simple microtubule arrays with discrete functions during the cell cycle (Kilmartin and Adams, 1984; Jacobs et al., 1988), and many of the components of the yeast MTOC, the spindle pole body (SPB), are conserved with other eukaryotes (Murphy et al., 1998; Tassin et al., 1998).

Yeast γ-tubulin is a 473 amino acid essential protein encoded by the *TUB4* gene (Sobel and Snyder, 1995). Tub4p is located at the SPB (Sobel and Snyder, 1995; Marschall et al., 1996; Spang et al., 1996) and associates with two other highly conserved components of the yeast γ-tubulin complex (Spc97p and Spc98p; Rout and Kilmartin, 1990; Geissler et al., 1996; Knop et al., 1997). Many temperature-sensitive *tub4* mutants fail to form microtubules (Marschall et al., 1996), suggesting that Tub4p is essential for microtubule nucleation in vivo. Tub4p contains a highly conserved motif, DSYL, in its carboxy terminus. Deletion of this domain reveals that it is important for proper microtubule organization (Vogel and Snyder, 2000).

In this study, we investigate whether Tub4p is modified in vivo, as well as the role of modification during the cell cycle. We demonstrate that Tub4p is phosphorylated in vivo, and that phosphorylation is maximal during G1. One site of phosphorylation was mapped to Tyr445 of the DSYL motif, a conserved domain required for proper microtubule organization (Vogel and Snyder, 2000). Mutation of Tyr445 to Asp, which mimics phosphorylation, results in a temperature-sensitive *tub4* allele. *tub4-Y445D* cells arrest prior to anaphase, suggesting dephosphorylation of Tyr445 is required for mitosis. We show that the frequency of microtubule assembly at the SPB region and the number of astral microtubules per cell are increased in *tub4-Y445D* cells. The length of the anaphase spindle increases in *tub4-Y445D* cells, suggesting that the intranuclear microtubules are also affected. Astral microtubules are predominantly directed into the mother cell and transient spindle displacement is frequently observed in *tub4-Y445D* cells. Together, these results demonstrate that modification of γ-tubulin is important for controlling microtubule assembly and number, and thereby affects microtubule organization and function during the yeast cell cycle.

Results

Tub4p Is a Phosphoprotein In Vivo

Previous studies using conventional one-dimensional gels have not revealed multiple isoforms of γ-tubulin. We therefore investigated whether Tub4p is modified in vivo using two-dimensional (2D) gel electrophoresis. For these experiments, it was critical to have protein phosphatase inhibitors (PPase inhibitors; β-glycerophosphate, NaF, and o-vanadate) to detect the acidic isoforms. Proteins from asynchronous cells containing the *TUB4* ORF and promoter region on a high copy 2 micron plasmid were separated in 2D gels, and Tub4p isoforms were detected in immunoblots with antibodies directed

[3] Correspondence: michael.snyder@yale.edu

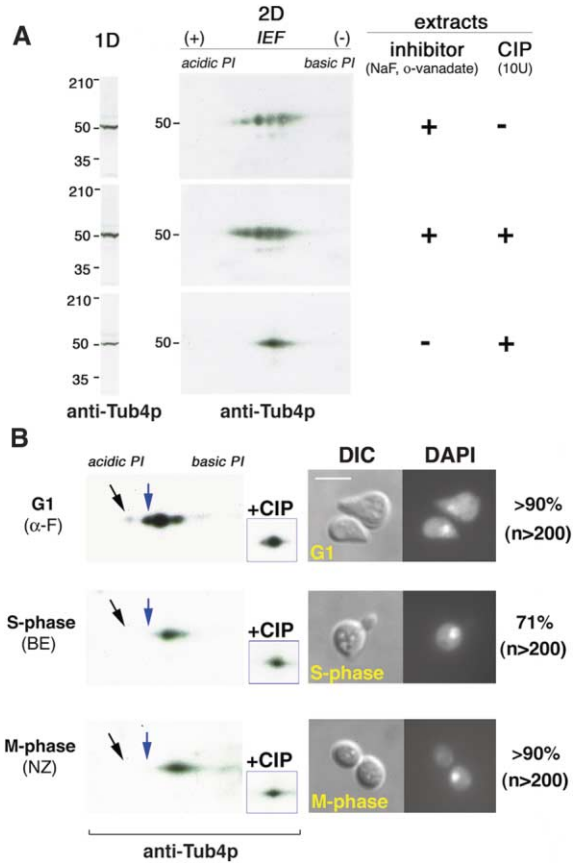

Figure 1. Tub4p Is Differentially Phosphorylated In Vivo

Tub4p is phosphorylated (A) in vivo. Extracts were prepared from asynchronous *tub4::HIS3* cells containing a 2 micron *TUB4* plasmid and incubated in the presence of PIC (phosphatase inhibitor cocktail: 10 mM NaF, 1 mM o-vanadate, and 20 mM β-glycerophosphate), PIC and CIP, or CIP alone. Tub4p isoforms were analyzed in 2D gels as described in Experimental Procedures. Anti-Tub4p$^{N\text{-}term}$ antibodies detect five isoforms in extracts treated with PIC or PIC and CIP, but a single isoform is detected in extracts treated with CIP alone. Tub4p is differentially phosphorylated during the yeast cell cycle (B). Extracts were prepared from wild-type cells in G1, S phase, and M phase. Tub4p isoforms were examined in analytical 2D gels. Tub4p has multiple isoforms in G1; a single isoform is detected when extracts are treated with CIP. Acidic isoforms of Tub4p (arrows) are not detected in S phase or M phase. Treatment with CIP has no significant effect on Tub4p isoform mobility in S phase or M phase, suggesting that Tub4p is dephosphorylated in these cells. Examples of representative cells for each phase of the cell cycle. The scale bar in (B) indicates 5 μm.

to the N terminus of Tub4p. As shown in Figure 1A, five discrete Tub4p isoforms are detected by anti-Tub4p antibodies.

To determine whether Tub4 is modified by phosphorylation, the inhibitors were left out and the extract was treated with calf intestinal phosphatase (CIP); under these conditions, only a single isoform that corresponds to the most basic species was detected. Conversely, all the acidic isoforms are detected in CIP-treated samples containing phosphatase inhibitors (Figure 1A). Similar results are obtained using endogenous levels of Tub4p; however, the two most acidic isoforms are present, but with low abundance and are therefore difficult to observe (see following section). These data provide evidence that a γ-tubulin (Tub4p) is phosphorylated in vivo.

Phosphorylation of Tub4p Is Cell Cycle Dependent

We next examined whether Tub4p phosphorylation changes during the yeast cell cycle. Wild-type cells containing endogenous levels of Tub4p were arrested in G1 with α factor (Minshull et al., 1996) and released into fresh medium in the presence and absence of nocodozole (NZ), a microtubule-destabilizing drug that arrests cells prior to mitosis (Jacobs et al., 1988; Minshull et al., 1996). Lysates were prepared from cells in G1, S phase (coincident with bud formation), and M phase, extracted in the presence of PPase inhibitors or with CIP, and subsequently incubated at 37°C for 30 min, and the proteins were prepared for 2D gel analysis (Figure 1B). Representative cells from each phase are shown. At least four Tub4p isoforms are detected in extracts prepared from G1-arrested cells. As before, treating extracts with CIP eliminates all of the acidic isoforms and results in a single basic isoform. The acidic Tub4p isoforms are dramatically reduced in extracts prepared from S phase cells (as indicated by bud formation) and absent in M phase cells. Treatment with CIP had little effect on Tub4p isoform complexity or mobility in S phase and M phase samples. Overexposure of these samples did not reveal additional isoforms (data not shown). Together, these results indicate that Tub4p phosphorylation occurs predominantly in G1 and is absent in mitosis.

Tyr445 Is Required for Phosphorylation In Vivo

The carboxy terminus (CTR) of Tub4p is composed of the conserved DSYL motif and divergent acidic tail region. The DSYL motif is highly conserved between Tub4p and yeast α-tubulins (Tub1p and Tub3p), but not yeast β-tubulin (Tub2p). The Tyr445 and nearby Ala439, Ala440, and Leu446 residues are also highly conserved in γ-tubulins (NCBI/Blast; consensus motif: AAE/T---YL/I); the Y445 residue is invariant in all known γ-tubulin sequences (Figure 2A). Deletion of the DSYL motif significantly affects microtubule organization (Vogel and Snyder, 2000), raising the possibility that these residues serve to regulate the CTR's role in microtubule organization. Thus, we speculated that modification of one or more of these residues might be regulated by phosphorylation to control microtubule organization.

We constructed a series of Tub4 mutants in which either the Ser444 (S444) or Tyr445 (Y445) were substituted for nonphosphorylatable residues (Ala and Phe) or residues that mimic phosphorylation (Asp). These alleles were introduced into the chromosome for expression at endogenous levels (see Experimental Procedures). Since mutations in Tyr445 have phenotypic consequences (see following sections), we focused in particular on whether Tyr445 is modified during G1 of the cell cycle in vivo. Wild-type and *tub4-Y445F* cells were arrested in G1 with α factor, released from the arrest, and the proteins were prepared at 30 min after release (when cells are in late G1, 10 min prior to bud emergence; data not shown). As shown in Figure 2B, two Tub4p isoforms are in wild-type extracts 30 min postrelease; in contrast, a single Tub4p isoform was detected in *tub4-Y445F* extracts 30 min postrelease (Figure 2B). Longer exposures of these samples saturated the film but did not reveal other isoforms (data not shown). Finally, protein samples were prepared from asynchronous cells overexpressing

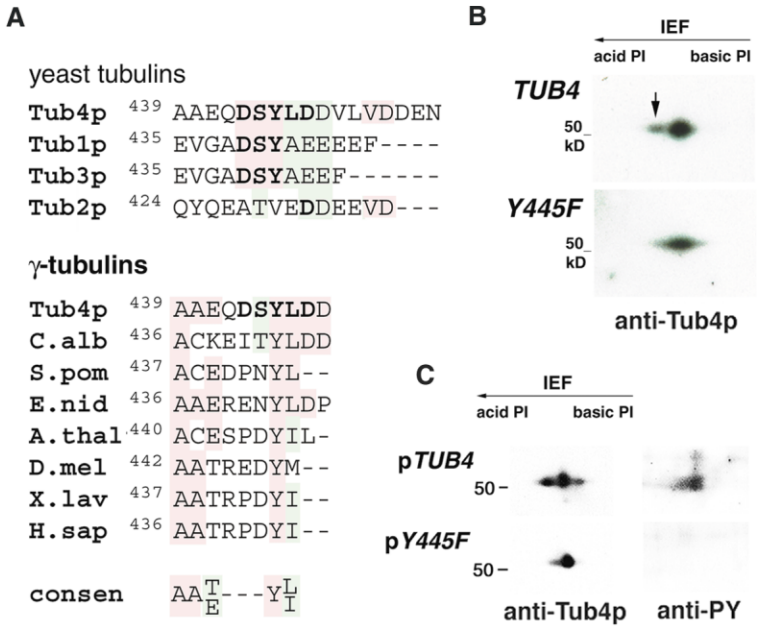

Figure 2. Tyr445 Is Phosphorylated In Vivo

Tub4p has an acidic carboxy terminus that contains the DSYL motif (residues 443–446), which are conserved between yeast α- and γ-tubulins but not β-tubulin. Residues Ala439 and Ala440 are highly conserved and Tyr445 is invariant in all γ-tubulins (A). Whole-cell extracts were prepared from wild-type or *tub4-Y445F* cells just prior to bud emergence (30 min postrelease from α factor arrest) in the presence of PIC. Tub4p isoforms were analyzed in 2D gels with anti-Tub4p$^{N\text{-}term}$ antibodies. In wild-type extracts, two Tub4p isoforms are detected at 30 min after release; one major Tub4p isoform is detected in extracts prepared from the *tub4-Y445F* mutant (B). Protein samples were prepared in the presence of the tyrosine PPase inhibitor o-vanadate from asynchronous cells overexpressing wild-type or the Tyr445→Phe mutant protein from high copy plasmids. An anti-phosphotyrosine antibody stains wild-type but not Tyr445→Phe Tub4p isoforms (C).

wild-type or the Tyr445→Phe mutant protein from 2 micron plasmids in the presence of the tyrosine PPase inhibitor o-vanadate. An anti-phosphotyrosine antibody stains the wild-type but not the mutant Tub4p isoforms (Figure 2C). Thus, Tyr445 is required for one Tub4p phosphorylation event in G1 of the cell cycle.

Tyr445 Is Important for Tub4p Function

We next examined the consequences of mutating Tyr445 to either phenylalanine or aspartate. As controls, Ser444 was changed to alanine or aspartate (or Ser444 or Tyr445 to lysine). All mutations were introduced into the *TUB4* chromosomal locus in diploid cells by homologous recombination and confirmed by DNA sequencing. Haploid segregants of heterozygous diploids were tested for growth defects at 25°C, 34°C, 37°C, and 13°C. Strains containing mutations at Ser444 (Ser444Ala, Ser444Asp, and Ser444Lys), Tyr445Phe, and Tyr445Lys did not exhibit growth defects at any of the temperatures tested. However, we found that cells containing the Tyr445Asp mutation (*tub4-Y445D*) did not form colonies at 34°C or 37°C (Figure 3A). The majority of *tub4-Y445D* cells incubated on solid medium at the restrictive temperature (37°C) for ~24 hr form colonies when shifted back to the permissive temperature (25°C), indicating that these cells remained viable at 37°C (Figure 3B). Analysis of DNA content by fluorescent activated cell sorting analysis revealed that *tub4-Y445D* cells incubated at the restrictive temperature have replicated their DNA (data not shown). The viability of *tub4-Y445D* cells is dependent on the *MAD1* gene product, which is required for the spindle assembly checkpoint (Li and Murray, 1991; Hoyt, 2001). When *tub4-Y445D* and *mad1*Δ strains are mated and diploids are sporulated, the majority of tetrads examined (79%, n = 16) contain one dead spore, and only 2% of the viable progeny recovered are *tub4-Y445D mad1*Δ double mutants (Figure 3C).

Since the growth defects of *tub4-Y455D* cells might arise from reduced protein levels at a restrictive temperature (34°C), extracts were prepared from wild-type and *tub4-Y445D* cells and probed for Tub4p by immunoblot analysis. Yeast β-tubulin (Tub4p) was used as a total protein loading control and detected in extracts with anti-Tub2p antibodies (Bond et al., 1986). Similar levels of wild-type, mutant protein, and Tub2p were observed in each strain, indicating that the observed growth defect of *tub4-Y445D* cells is not due to reduced levels of protein (Figure 3D).

The normal γ-tubulin complex of budding yeast contains two molecules of Tub4p (Knop et al., 1997). We tested whether the mutant protein is capable of forming a Tub4-Y445Dp-Tub4-MYCp complex using coimmunoprecipitation experiments using anti-MYC or anti-Tub4p antibodies. As shown in Figure 3E, Tub4p is not detected in immunoprecipitations prepared from untagged wild-type extracts; in contrast, the Tub4-MYCp fusion protein is detected in extracts prepared from *TUB4::MYC/TUB4::MYC* and *TUB4::MYC/tub4-Y445D* strains. The untagged mutant protein coimmunoprecipitates with Tub4-MYCp, indicating that it assembles into the Tub4p complex (Figure 3E). Thus, the growth defect of the *tub4-Y445D* mutant is not due to an inability to form a Tub4p-Tub4p complex.

We next investigated whether phosphorylation of Tyr445 might regulate Tub4p function by examining the effect of the *tub4-Y445D* mutation on nuclear positioning and microtubule organization when cells are incubated at the restrictive temperature. Cells were arrested in G1with α factor (Figure 4A, panels a′ and c′) and released into prewarmed media and incubated for 2 hr at 34°C. Cell morphology and nuclear position were monitored at 40 min postrelease from the arrest, and every 20 min thereafter (Figure 4C). At least 200 cells were examined per strain per time point. Bud formation occurred at 40 min postrelease in the majority (>70%) of wild-type, *tub4-Y445D*, and *tub4-Y445F* cells and by 60 min, 98% of wild-type and 90% of *tub4-Y445D* and *tub4-Y445F* cells had large buds and the nucleus was positioned at or near the bud neck (Figure 4C). After 2 hr incubation at the restrictive temperature, the majority

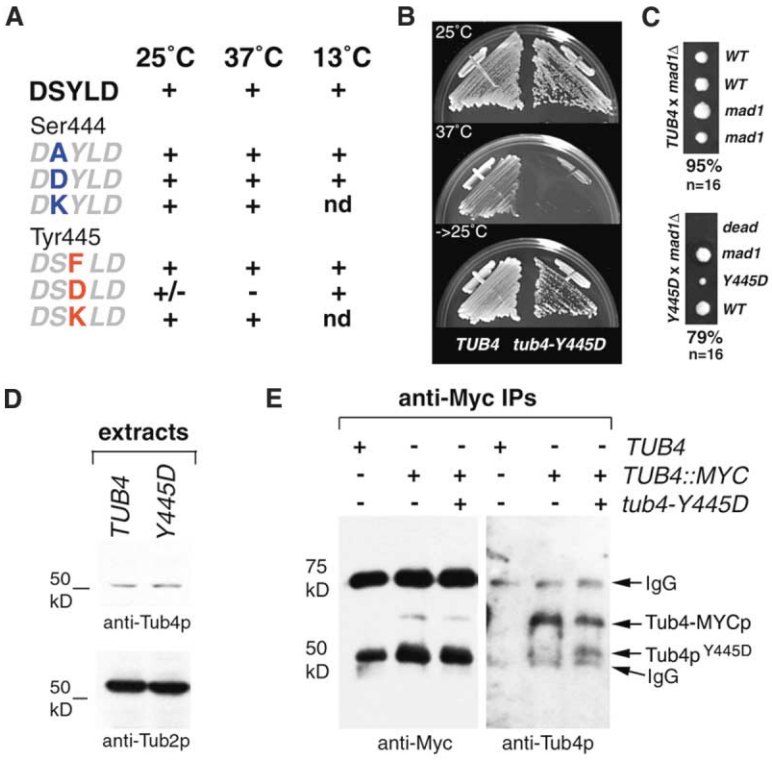

Figure 3. Analysis of DSYL Point Mutations

Amino acid substitutions were created in Ser444 and Tyr445 by site-directed mutagenesis and were integrated into the *TUB4* locus; *TRP1* was used to mark these alleles (see Experimental Procedures). Only one mutation (*tub4-Y445D*) was found to have a phenotype, a conditional growth defect at 37°C (A). *tub4-Y445D* cells recover from incubation (>16 hr) at the restrictive temperature, suggesting lack of growth is a result of cell cycle arrest/delay rather than inviability (B). *tub4-Y445D* is colethal with *mad1*Δ, demonstrating that Mad1p is required for viability (C). The mutant Tub4p^{Y445D} protein is not depleted in extracts prepared from cells incubated at a restrictive temperature (34°C) (D). The mutant protein forms a Tub4-Y445Dp-Tub4-MYCp complex, as shown by its coimmunoprecipitation with a functional Tub4-MYCp fusion protein (E). Neither the wild-type nor mutant protein is immunoprecipitated by anti-Myc antibodies (data not shown).

of wild-type cells have formed a second bud (>60%; the remainder of cells were unbudded), indicating completion of one cell cycle (Figure 4A, panel b′). In contrast, the majority of *tub4-Y445D* cells remain large budded with the nucleus at or in the bud neck (Figure 4A, panel d′). The mother cells are much larger than in the wild-type strain.

Microtubules were examined in wild-type and *tub4-Y445D* cells after 2 hr of incubation at 34°C (Figure 4B). Fixed cells were stained with YOL1/34, a rat monoclonal antibody raised against yeast α-tubulins (Tub1/3p), and detected with an FITC-anti-rat IgG conjugate. The majority of wild-type cells (either unbudded or with a small bud) have one or two bright foci of tubulin staining as detected by indirect immunofluorescence with α-tubulin antibody (Figure 4B, panel b′, arrows). The majority of *tub4-Y445D* cells have preanaphase spindles (~2 μm in length); however, many of the spindles are bent (Figure 4B, panel d′, arrows). Together, these data indicate that *tub4-Y445D* cells arrest prior to anaphase with a bipolar spindle.

The *tub4-Y445D* Mutation Promotes Astral Microtubule Assembly and Growth

To investigate whether the *tub4-Y445D* mutation alters microtubule number and/or stability, we examined astral microtubules in living cells; these experiments demonstrated that more microtubules are assembled from the region of the SPBs in *tub4-Y445D* cells. Microtubule assembly, number, and dynamics were analyzed in two independent wild-type or *tub4-Y445D* strains expressing a *TUB1::GFP* fusion integrated at the *URA3* locus (Straight et al.,1997) by time-lapse video microscopy (Shaw et al., 1997). Astral microtubules were examined in small budded cells in which the spindle was located at or near the neck of the bud at the start of the time course (as was the case for the majority of wild-type and *tub4-Y445D* cells). These cells have already migrated their nucleus properly, indicating that the astral microtubules are functional (Shaw et al., 1997; Miller and Rose, 1998), are not delayed or arrested as a result of the spindle assembly checkpoint, and are expected to have dephosphorylated Tub4p.

To examine the effect of the *tub4-Y445D* mutation on microtubule assembly, we measured the frequency at which new microtubules appear in the region of the SPBs. Importantly, the frequency at which new microtubules emanating from the region of the SPBs become visible (i.e., nucleation or regrowth from existing short microtubules) is significantly increased in *tub4-Y445D* cells (0.6 ± 0.05 microtubules assembled/min) relative to wild-type cells (0.4 ± 0.03 microtubules assembled/min; Table 1). In addition, similar to CTR truncations (Vogel and Snyder, 2000), the number of astral microtubules per cell increases in *tub4-Y445D* cells (2.7 ± 0.08, n = 8) relative to wild-type cells (1.5 ± 0.07, n = 8; Table 1). Together, these results suggest that the *tub4-Y445D* mutation promotes the assembly of astral microtubules.

The dynamics of astral microtubules might also be altered as a result of the increased number of microtubules observed in *tub4-Y445D* cells. We therefore measured the elongation and shortening rates of astral microtubules in wild-type (n = 8 cells, 8 microtubules) and *tub4-Y445D* (n = 6 cells, 13 microtubules) cells. The elongation rate of microtubules was similar in wild-type (1.03 ± 0.103 μm/min) and *tub4-Y445D* (1.20 ± 0.140

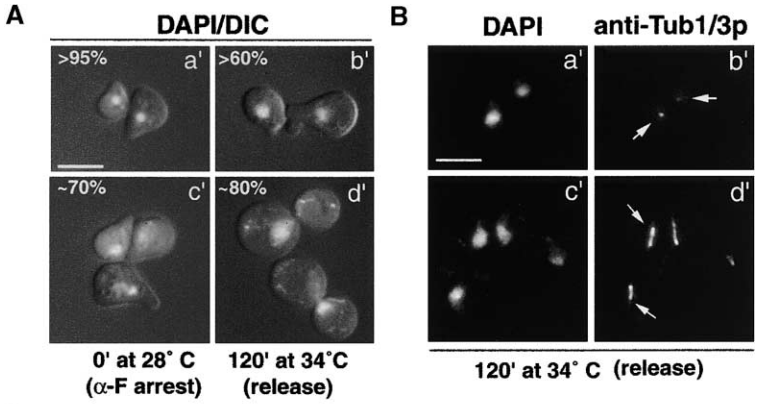

C

strain	time (minutes) post-release	>95	>70			I	II
TUB4 (n=201)	0	>95					
	40		>70				
	60			2	98	0	
	80			1	11	89	(II)
	100	85		1	0	15	
Y445D (n=264)	0	>95					
	40		~70				
	60			9	91	0	
	80			5	83	15	
	100	3		2	51	44	(I)
Y445F (n=312)	0	>95					
	40		>70				
	60			8	92		
	80			9		90	(II)
	100	90				10	

Figure 4. *tub4-Y445D* Cells Arrest Prior to Anaphase

Wild-type and *tub4-Y445D* cells were arrested in G1 with α factor at 28°C ([A], panels a′ and c′), released from the arrest, and incubated for 2 hr at 34°C. Cell morphology was monitored at 40 min postrelease (bud formation) and every 20 min thereafter (C). At least 200 cells were examined per strain. *tub4-Y445D* cells arrest with a migrated nucleus and large bud (A). Wild-type cells complete one cell cycle and have formed a new bud after 2 hr ([A], panel b′). The terminal arrest phenotype of *tub4-Y445D* cells is large budded with a nucleus positioned at or in the bud neck ([A], panel d′). Microtubules in these cells were examined by indirect immunofluorescence with anti-Tub1/3p antibodies (B). One or two foci of tubulin staining is observed in the majority of wild-type cells ([B], panel b′, arrows); in contrast, the majority of *tub4-Y445D* cells have preanaphase spindles (~2 μm in length), and the spindles appear bent ([B], panel d′, arrows). The timing of bud emergence and nuclear migration is similar for wild-type, *tub4-Y445D*, and *tub4-Y445F* strains (C). Less than 10% of *tub4-Y445D* and *tub4-Y445F* cells have their nucleus in the mother cell 60 min after release from α factor arrest. The scale bars in (A) and (B) = 5 μm.

μm/min) cells (Table 1); however, microtubules depolymerized faster in *tub4-Y445D* cells (1.59 ± 0.193 μm/min) relative to those in wild-type cells (1.18 ± 0.125 μm/min; Table 1). Additionally, the average period of elongation was significantly longer in *tub4-Y445D* cells (65.3 ± 8.25 s) than in wild-type cells (42.8 ± 4.53 s). In agreement with this observation, we found the average maximal length of the astral microtubules also increased in *tub4-Y445D* cells (2.3 ± 0.15 μm) relative to wild-type cells (1.6 ± 0.14 μm; Table 1).

Taken together, these latter results suggest that the transition between microtubule elongation and pausing or catastrophe is inhibited in *tub4-Y445D* cells. However, not all astral microtubules in *tub4-Y445D* cells exhibit suppressed dynamics. We observed that one of several microtubules in the same *tub4-Y445D* cell exhibited normal dynamics, such as a pause during elongation or a shorter elongation phase, whereas the others have abnormal kinetics. Examples of microtubule dynamics in a wild-type cell and a *tub4-Y445D* cell are shown in Figure 5. In the wild-type cell (Figure 5A), the microtubule elongates for 41 s, shortens for 20 s, and then elongates for a further 61 s before the next catastrophe event. Two of the three microtubules in the *tub4-Y445D* cell elongate for an extended period of time (>80 s); however, a third pauses after 20 s of growth, elongates for another 40 s, and then shortens (Figure 5B). Thus, the effect of the *tub4-Y445D* mutation on astral microtubule growth is not global, and perhaps is due to increased numbers of microtubules competing for

Table 1. Assembly Rate, Number, and Dynamics of Tub1:GFP-Labeled Astral Microtubules

Strain	Microtubules assembled† (per min)	Astral microtubules (per cell)	Astral microtubule dynamics: Elongation rate μm/min	Shortening rate μm/min	Elongation phase (s)	Microtubule length (max; μm)
TUB4	0.4 ± 0.03	1.5 ± 0.07	1.03 ± 0.103	1.18 ± 0.125	42.8 ± 4.53	1.6 ± 0.14
Y445D	0.6 ± 0.05	2.7 ± 0.08	1.20 ± 0.140	1.59 ± 0.193	65.3 ± 8.25	2.3 ± 0.15
	$p < 0.01$	$p < 0.01$		$p < 0.01$	$p < 0.05$	$p < 0.01$

Astral microtubules were examined in small budded cells with a spindle at or near the neck at t = 0. Cells were observed for 12–15 min at 25°C. Frequency at which new microtubules appeared at the SPBs (*TUB4*, n = 8 cells; *Y445D*, n = 12 cells), number (*TUB4*, n = 8 cells; *Y445D*, n = 8 cells), elongation/shortening rates, and average maximum length (*TUB4*, n = 8 cells, 8 microtubules; *Y445D*, n = 6 cells, 13 microtubules) were determined as described in Experimental Procedures.

† Number of new microtubules (resulting from either nucleation or regrowth) visible in the region of the SPBs per unit time.

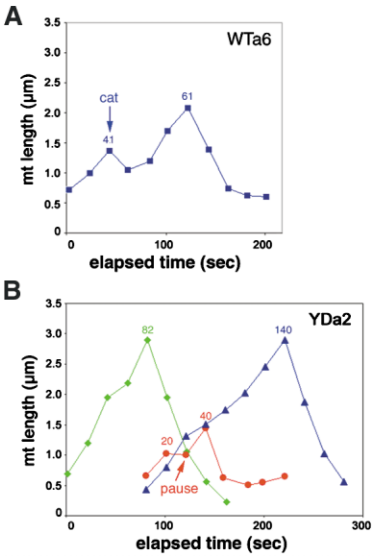

Figure 5. A Subset of Microtubules Exhibit Normal Dynamics in *tub4-Y445D* Cells

Astral microtubules in wild-type cells typically undergo frequent transitions from growth to a paused or catastrophe state. An example of this in a wild-type cell is shown in (A). In the majority of *tub4-Y445D* cells, several astral microtubules can be monitored simultaneously; an example is shown in (B). The transition from growth to pause or catastrophe is suppressed in two astral microtubules, resulting in a prolonged elongation phase and increased maximal length (B). However, a third microtubule undergoes a pause after 20 s of growth, and then resumes elongating. This analysis indicates that the effect of the *tub4-Y445D* mutation on astral microtubule dynamics is not global, and is likely to be indirect.

limited factors that contribute to microtubule dynamics (see Discussion).

Increased Microtubule Assembly in *tub4-Y445D* Cells Causes Defects in Microtubule Organization

The frequency of microtubule assembly and the number of astral microtubules are increased in *tub4-Y445D* cells. The rapid formation of these astral microtubule arrays might affect their direction of termination and bud or bud neck cortex (mt_b) versus mother cell cortex (mt_m), and thereby affect spindle position. We determined the percentage of newly assembled mt_b and mt_m in wild-type and *tub4-Y445D* cells. In small budded wild-type cells with a spindle positioned at the neck, >50% of astral microtubules grow into and terminate in the bud, whereas only 23% terminate in the mother cell. In contrast, ~50% of astral microtubules grow into and terminate in the mother cell in *tub4-Y445D* cells (Figure 6A).

The mt_b exert pulling force on the spindle, whereas the mt_m exert pushing force (Adames and Cooper, 2000). These opposing forces act to maintain spindle position at the bud neck until spindle elongation occurs (Yeh et al., 2000). The number of mt_m increases in *tub4-Y445D* cells; we observed that mt_m transiently displaced the spindle from the neck in the majority of *tub4-Y445D* cells examined. An example of spindle displacement is shown in Figure 6B. At the start of the time lapse, an mt_b (t = 0:00) pulls the spindle toward the neck (t = 0:22) and orients it (t = 1:42). Subsequently, an mt_m forms (t = 2:42) and elongates, displacing the spindle from the neck (t = 5:21, left arrow). A second mt_m rotates the spindle perpendicular to the *z* plane (t = 5.21, right arrow). Eventually, these microtubules shorten and the spindle repositions at the bud neck (t = 8:02–14:42). Spindle displacement and subsequent reorientation were not observed in any of the wild-type cells examined (n = 8), but were observed in 75% of *tub4-Y445D* cells (n = 12).

The function of the spindle microtubules is likely to be affected by the *tub4-Y445D* mutation. Cells with a medium-sized bud and a spindle <2 μm in length were imaged at 1 min intervals for ~2 hr (see Experimental Procedures). In wild-type and *tub4-Y445D* cells, the spindle elongates into the bud and mother cell (Figure 6C). In wild-type cells, the length of the anaphase spindle (~8 μm) extends the length of the cell (ratio = 1.0 ± 0.02) before spindle breakdown (Figure 6C). In contrast, the spindle length in *tub4-Y445D* cells is greater than the length of the cell, forming a "fish hook" anaphase spindle with curved ends (Figure 6C). The ratio of the spindle length relative to the length of the cell revealed that the normalized maximal spindle length significantly increased in *tub4-Y445D* cells (1.2 ± 0.04, $p < 0.01$) compared to wild-type cells (1.0 ± 0.02). The elapsed time between the onset of anaphase and spindle breakdown was not significantly altered in *tub4-Y445D* cells (Figure 6C). Thus, the *tub4-Y445D* mutation appears to affect the growth and organization of astral and intranuclear microtubule arrays.

The *tub4-Y445D* Mutation Is Dominant for Resistance to Benomyl

The analysis of microtubule assembly, number, and dynamics in *tub4-Y445D* cells indicates that they have enhanced microtubule arrays. This observation predicts that the *tub4-Y445D* strain should be resistant to microtubule depolymerizing drugs. We therefore tested the growth of wild-type and *tub4-Y445D* cells in the presence of benomyl, a microtubule depolymerizing drug. Wild-type and mutant strains were tested for resistance and/or sensitivity to 10 μg/ml benomyl at 25°C. Haploid *tub4-Y445D* (Figure 7A) and diploid *TUB4/tub4-Y445D* (Figure 7B) cells are resistant to benomyl relative to wild-type cells. The conditional growth defect at 34°C is not observed for the heterozygous strain or for haploid mutant strains containing a *TUB4* centromeric plasmid (data not shown). The benomyl-resistant phenotype observed for homozygous and heterozygous *tub4-Y445D* strains suggests that *tub4-Y445D* is a semidominant activating mutation that increases microtubule number and/or stability.

Discussion

Previous studies of γ-tubulins have concentrated on the identification and characterization of proteins that associate with γ-tubulins (Zheng et al., 1995; Knop and Schiebel, 1997, 1998; Nguyen et al., 1998; Oegema et al., 1999; Gunawardane et al., 2000; Zhang et al., 2000) or how γ-tubulin is positioned at the minus end of the microtubule (Moritz et al., 2000; Wiese and Zheng, 2000; Keating and Borisy, 2000). The data presented above

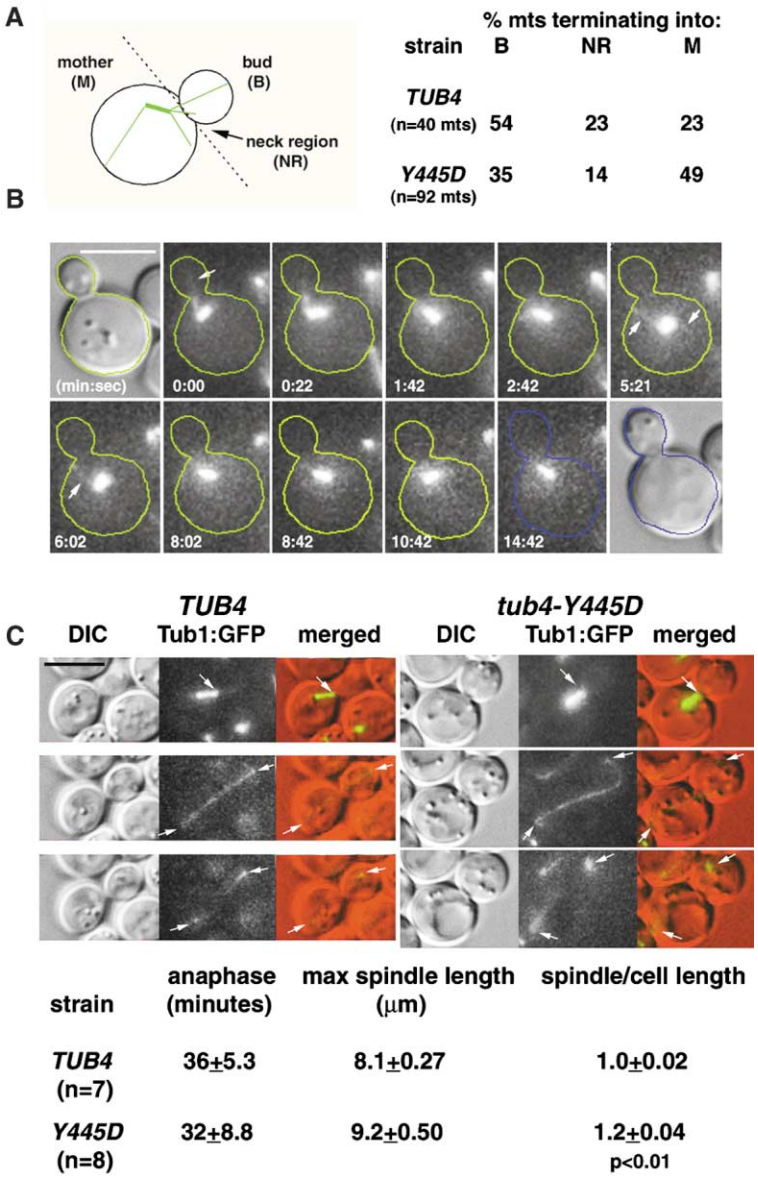

Figure 6. Microtubule Organization Is Altered in *tub4-Y445D* Cells

The percentage of microtubules terminating in the mother cell increases in *tub4-Y445D* cells relative to wild-type cells (A). Spindles are frequently displaced from the bud neck and microtubules terminating in the mother cell contribute to the loss of spindle position. Cell borders are shown as green (last time point is blue) outlines. Arrows indicate astral microtubules (B). The spindle frequently curves during anaphase in *tub4-Y445D* cells, forming a "fish hook" spindle (C). Corrected anaphase spindle length (spindle length/cell length) is increased in *tub4-Y445D* cells. Scale bars indicate 5 μm.

represents an in vivo examination of γ-tubulin (Tub4p) regulation during the cell cycle. We demonstrate that Tub4p is a phosphoprotein; it is hyperphosphorylated in G1 and dephosphorylated during mitosis. One G1-specific phosphorylation is dependent on a highly conserved tyrosine residue. Only a few examples of tyrosine phosphorylation (one example being phosphorylation of Cdc28p by Swe1p) have been reported previously in yeast (Amon et al., 1992; Sorger and Murray, 1992), suggesting that this form of modification is rare (see Zhu et al., 2000; Modesti et al., 2001). The timing of phosphorylation of Tub4p is different from that of Spc98p. Phosphorylation of Spc98p peaks after bud emergence and appears to play a role in its nuclear compartmentalization (Pereira et al., 1998).

What is the role of Tub4p phosphorylation? Tub4p phosphorylation appears to regulate microtubule assembly, and thereby affects microtubule number, stability, and organization. In support of this hypothesis, we find that the frequency of new microtubules detected at the SPBs and the number of astral microtubules are increased in the *tub4-Y445D* mutant, which mimics constitutive phosphorylation. Phosphorylation of Tub4p during G1 is likely to be important for stimulating microtubule assembly during spindle pole duplication. This would lead to the formation of a full complement of microtubules from each pole as cells prepare for pole separation and mitosis. The *tub4-Y445D* mutation has a more pronounced effect on microtubule assembly and stability than the opposing *tub4-Y445F* mutation. Although the reasons for this are not known, we speculate that (1) phosphorylation of several Tub4p residues participates in promoting microtubule assembly in G1 (this is consistent with the detection of multiple acidic Tub4p isoforms in G1) and/or (2) dephosphorylation of Tub4p is critical for cell cycle progression. Dephosphorylation of Tub4p is presumably critical for mitosis.

tub4-Y445D cells arrest with short spindles at the bud

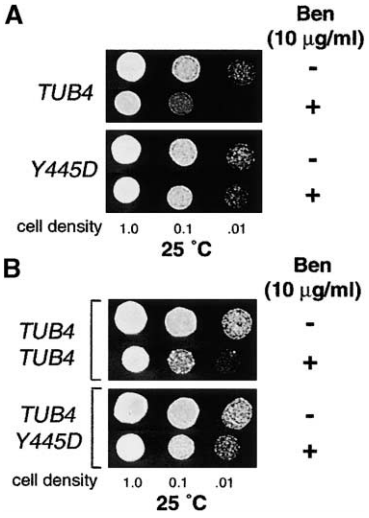

Figure 7. The *tub4-Y445D* Mutation Is a Semidominant Allele

Wild-type and mutant strains were tested for their ability to grow on YPAD containing 10 μg/ml benomyl. Serially diluted cultures were spotted (5 μl) on YPD supplemented with either DMSO (control) or benomyl. *tub4-Y445D* cells are resistant to benomyl relative to wild-type cells (A). Heterozygous *TUB4*/*tub4-Y445D* cells grow in the presence of benomyl; in contrast, the growth of wild-type diploid cells (heterozygous for the *TRP1* marker) is inhibited, demonstrating that *tub4-Y445D* is a semidominant allele (B).

neck and increased numbers of astral microtubules. Interestingly, these phenotypes are similar to those of cells in which the DSYL domain of the CTR has been deleted (Vogel and Snyder, 2000). The observed phenotypes of the *tub4-Y445D* mutant (increased assembly and number of microtubules, and dominant resistance to benomyl) suggest that it is a dominant activating mutation. The fact that a dominant active mutation that mimics phosphorylation and CTR deletions has similar effects on microtubule number and organization suggests that Tyr445 phosphorylation may inhibit the CTR. These data are consistent with the hypothesis that the CTR plays an inhibitory role in microtubule assembly and/or stability (Vogel and Snyder, 2000). Inactivation of this region during G1 by phosphorylation would therefore promote microtubule assembly.

How might phosphorylation of Y445 contribute to microtubule organization in the cell? We have demonstrated that the *tub4-Y445D* mutation increases the assembly rate of microtubules. The corresponding increase in microtubule number is correlated with a significant increase in the number of microtubules directed into the mother cell (see Figure 6A). Thus, we speculate that controlling the assembly of microtubules during the cell cycle is crucial for their proper organization and function. We observed that spindles often lose position from the bud neck in *tub4-Y445D* cells. This is likely to be the result of pushing forces exerted by mother-directed microtubules (Adames and Cooper, 2000) in the absence of pulling forces exerted by microtubules interacting with the bud or bud neck (Yeh et al., 2000). Bud tip and bud neck interactions are important for proper spindle positioning (Carminati and Stearns, 1997; Shaw et al., 1997) and maintaining the spindle at the neck prior to anaphase (Yeh et al., 2000). One possibility is that increasing the number of microtubules titers microtubule-associated factors (such as plus end binding proteins) regulating microtubule dynamics, resulting in spindle position/function defects and elongated astral and spindle microtubules.

These data suggest that modification of yeast γ-tubulin during the cell cycle is important for controlling microtubule number and organization. The Tyr445 residue of Tub4p is conserved within the carboxy terminal residues of many γ-tubulins, suggesting a general role of γ-tubulin modification in regulating microtubule organization in many organisms. Further studies to identify proteins that regulate Tub4p and/or the CTR will help provide important insights for understanding how microtubule organization is regulated during the cell cycle.

Experimental Procedures

Media and General Methods

Yeast cells were grown and manipulated using standard techniques (Guthrie and Fink, 1991). Recombinant DNA manipulations were performed as described (Sambrook et al., 1989). Yeast strains were transformed with plasmids or PCR fragments using the one step transformation method (Chen et al., 1992).

Construction of Mutant Strains and Genetic Analysis

DSYL mutants were made by PCR site-directed mutagenesis using mutagenic oligonucleotide primers and a 2.2 kb genomic KpnI/NsiI fragment containing the *TUB4* gene in pSK (pSK-TUB4; Stratagene). Gel-purified PCR products were digested with PstI and SacI, and cloned into pSK-TUB4::TRP1. Plasmids were sequenced to confirm that they contained the appropriate, rather than an undesired, mutation. Gel-purified HincII fragments composed of ~300 bp of 5′ *TUB4* coding sequence containing the desired mutation followed by 100 bp of UTR and the *TRP1* gene were transformed into the diploid strain Y270 and *TRP1*$^+$ colonies obtained. Correct integration into the *TUB4* locus and the presence of the desired mutation were confirmed by sequencing PCR products amplified from flanking regions of the *TUB4* ORF. Heterozygous diploids were sporulated and *TRP1*$^+$ progeny were obtained by tetrad analysis (20 tetrads per mutation). The *tub4-Y445D* conditional growth defect segregated with the *TRP1* marker in >95% of haploid progeny of *TUB4*/*tub4-Y445D* diploids.

For overexpression studies, a 2.2 kb genomic KpnI/NsiI fragment was subcloned into pRS424 (Sikorski and Hieter, 1989), creating a high copy 2 micron plasmid. Plasmids were introduced into a *tub4Δ::HIS3* shuttle strain using standard methods (Boeke et al., 1984). The loss of the wild-type gene was confirmed by PCR.

MAD1 was disrupted in the diploid strain Y270 with URA3 flanked by 75 bp of the 5′ and 3′ regions of the *MAD1* ORF, integrated into the *MAD1* locus, and the disruption was confirmed by PCR and sensitivity to benomyl. Haploid *mad1Δ* segregants were obtained by tetrad dissection.

Preparation of Cell Cycle-Arrested Cells

Cells in were arrested in G1 with α factor (5 μg/ml) or in M phase with nocodozole (20 μg/ml) as previously described (Minshull et al., 1996; Pereira et al., 1998). Strains were grown overnight in liquid yeast peptone extract (YPD) and grown at 30°C to a density of ~1 OD^{600}. Cells were resuspended at a density of 0.3 OD^{600} in fresh YPD, grown for 90 min (~1 cell cycle), and then incubated with α factor at 30°C. After 1 hr, a second aliquot of α factor was added and incubated until greater than 90% of the cells (~200 cells counted) had formed mating projections. Cells were then pelleted at 1000× g and gently resuspended in fresh YPD with or without nocodozole. Bud morphology and nuclear position was assayed to confirm the arrest (~200 cells/condition/strain).

Light and Immunofluorescence Microscopy

For cytological studies, cultures were grown in rich medium to ~1 OD_{600} density at 25°C, synchronized with α factor as previously described, and incubated in fresh medium without α factor for 2 hr at either 28°C or 34°C. Cells were fixed with 3.7% formaldehyde for 30–40 min at ambient temperature. Fixed cells were incubated for 5 min in 0.2% 4′,6-diamidino-2-phenylindole-dihydrochloride (DAPI)/PBS to stain DNA, washed once with PBS, and mounted in 90% glycerol/2% n-propylgallate/PBS and examined with a Leica Aristoplan microscope. Cells were prepared for indirect immunofluorescence using previously described methods (Guthrie and Fink, 1991) and incubated with rat monoclonal antibody YOL1/34 (raised against yeast α-tubulin; SeraLab) and subsequently with FITC-conjugated goat anti-rat IgG (Jackson Immunologicals) to label microtubules. To visualize microtubules, cells were examined using an FITC filter with a 100× 1.32 NA objective. Images were captured using a Princeton Micromax CCD camera and Scanalytics IPLab software.

Time-Lapse Video Microscopy and Data Analysis

Microtubule number, length, and dynamics were examined in two independent *TUB4* and *tub4-Y445D* strains expressing *TUB1::GFP* (Straight et al., 1997). Cells were grown overnight at 24°C to mid-log phase. To measure astral microtubules, cells were mounted on 7% agar pads as previously described (Shaw et al., 1997). Observations were made at ambient temperature (24°C–25°C). Images were acquired using a Hamamatsu Orca II CCD camera (model C4742-98) mounted on an Eclipse E600FN using a 100× 1.4 NA Plan Apochromat objective lens with 1× magnification to the camera. Cells were typically observed for 12–15 min at 20 s intervals. At each time point, a z series composed of five optical sections (0.25 s GFP fluorescence images) taken at a z interval of 0.75 μm. A differential interference contrast (DIC) image was acquired at the start and end of each time course to monitor bud size and position. To measure maximal anaphase spindle length, cells were mounted on 25% gelatin pads. Medium budded cells with a spindle <2 μm in length were imaged with five 0.25 s GFP fluorescence images (z = 0.75 μm) acquired at 1 min intervals for ~2 hr. A single 0.25 s DIC image was taken at the midpoint of each *z* series.

Astral Microtubule Number

Microtubule number per cell was measured by counting the number of astral microtubules in each 20 s interval. The uncompiled 5-plane *z* series for each interval was used in order to count all microtubules regardless of length. The number of microtubules per interval was determined for the first 5 min of each time lapse and the average was determined for aggregate data collected from 8 cells. The variance and standard error for each data set and significance at $p < 0.05$ as determined by a two-tailed Student's t test was calculated with Excel software.

Frequency of Astral Microtubule Assembly and Direction

The frequency of new astral microtubule assembly (nucleation or regrowth) was determined by counting the number of assembly events during each time lapse/unit time. Assembly events were quantified using uncompiled 5-plane *z* series data from wild-type (n = 8) and *tub4-Y445D* (n = 12) cells. The direction of termination (mother, bud, and bud neck region) for each microtubule assembled was determined at the point of maximal length. The variance and standard error for each data set and significance at $p < 0.05$ as determined by a two-tailed Student's t test was calculated with Excel software.

Maximal Length and Dynamics of Astral Microtubules

The length and dynamics of astral microtubules in wild-type and *tub4-Y445D* cells was determined by measuring the length of single microtubules over time. Microtubule length was measured as x,y,z pixel units in calibrated, uncompiled 5-plane *z* series data in wild-type (n = 8 cells, 8 microtubules) and *tub4-Y445D* (n = 6 cells, 13 microtubules) cells using Measure Pixel software in Metamorph (Universal Imaging). Pixel measurement across the *x-y* and *z* planes was converted to μm, and the length per interval and rates of elongation (μm/min) and shortening (μm/min) were calculated with Excel software (macros provided by M. Gupta). The variance and standard error for each data set and significance at $p < 0.05$ as determined by a two-tailed Student's t test was calculated with Excel software.

Maximal Anaphase Spindle Lengths

The maximal corrected anaphase spindle length was determined using calibrated, compiled (merged) 5-plane *z* series data from wild-type (n = 7) and *tub4-Y445D* (n = 8) cells. The length of the cell (long axis through the bud neck) and the length of the spindle in the interval prior (~1 min) to the start of spindle breakdown was measured using Measure Regions software in Metamorph. The ends of the spindle were determined by the point to which the spindle depolymerized back to at the end of spindle breakdown. The variance and standard error for each data set and significance at $p < 0.05$ as determined by a two-tailed Student's t test was calculated with Excel software.

Preparation of Anti-Tub4p Antibodies

A KLH conjugate of a peptide corresponding to 16 N-terminal residues 107–122 of Tub4p (NGYDIGTRNQDDILNK) was used to generate polyclonal antibodies in rabbits (Zymed Laboratories). Total IgG was purified from rabbit sera with EZ-Sep (Pharmacia Biotech) and stored at −80°C. This antibody (1:3000) recognized a single ~52 kDa protein band in extracts prepared from cells expressing *TUB4* in high copy 2 micron plasmids (see Figure 2A).

Preparation of Extracts for Protein Analysis

Extracts were prepared using a modification of a previously described method (Knop et al., 1997). Yeast cultures were collected by centrifugation and cell pellets were washed with lysis buffer (1× lysis buffer: 200 mM NaCl, 1 mM EGTA, 5 mM $MgSO_4$, 50 mM Tris-HCl [pH 7.8], and 5% glycerol) containing 20 mM β-glycerophosphate and used directly or snap frozen and stored at −70°C. Cell pellets (20–100 μl) were suspended in two volumes of lysis buffer containing protease inhibitors (Sigma yeast protease inhibitor cocktail: 2 μg/ml benzamidine and 1 mM PMSF) and an equal volume of zirconium beads (Biospec Products) was added. Cells were disrupted by six 1 min pulses of vortexing at 4°C; this procedure was sufficient to break ~80% of the cells. Triton X-100 (10% in lysis buffer) and SDS were added to final concentrations of 2 and 0.1%, respectively, and lysates were extracted for 30–40 min on ice. Extracts were centrifuged at 6500× g for 12 min to clarify them. Clarified extracts used for immunoprecipitations were prepared with 1% Triton X-100 without SDS, and were diluted with an equal volume of 1× lysis buffer without salt or detergent before adding antibodies.

Protein Phosphatase Treatment of Extracts

Lysates (25 μl) were preincubated with either phosphatase inhibitors (1 mM ο-vanadate, 5 mM NaF, 20 mM β-glycerophosphate; phosphatase inhibitor cocktail; PIC) or buffer at 37°C for 15 min. Lysates were then incubated with buffer or 10 units (1 μl) of calf intestinal phosphatase (CIP) at 37°C for 30 min. The reaction was then quenched by the addition of an equal volume of lysis buffer containing 2× PIC, and Triton X-100 and SDS were added to 2% and 0.1%, respectively, and extracted on ice as previously described.

Two-Dimensional Electrophoresis

Extracts to be analyzed by two-dimensional electrophoresis (O'Farrell, 1975) were treated with RNase/DNase for 15 min on ice and centrifuged at 8000× g for 10 min. An aliquot (25 μl) of the supernatant was diluted with an equal volume of lysis buffer (without detergent), nine volumes of ice-cold acetone were added, and the proteins were precipitated for 2 hr at −20°C. Precipitated proteins were pelleted by centrifugation at 6000× g for 10 min, the acetone was removed, and the pellet was dried at room temperature. Protein pellets, representing ~25 μl of clarified extract, were solubilized in 50 μl of urea sample buffer (USB: 9.9 M urea, 2% Triton X-100, 5% β-mercaptoethanol, and 0.1% SDS containing 0.4% ampholytes). Samples were used immediately or stored at −80°C.

Two-dimensional electrophoresis was performed using a mini apparatus (Bio-Rad). Isoelectric focusing (IEF) gels (5 cm) containing either 5–7:3–10 (overexpressed proteins), 5–8:3–10 (cell cycle samples), or 4–6:5–7:3–10 (G1 samples) ampholyte mixtures were cast according to the manufacturer's instructions. IEF gels were prefocused at 200, 300, and 400 volts. Protein samples in USB were separated in IEF gels for 2800 volt hours (maximal voltage 750). After the focusing step, IEF gels were incubated in prewarmed (60°C)

2× SDS sample buffer (Laemmli, 1970) for 1 min, transferred to the top of a 3% stacking gel, and separated in 9% gels. Second dimension gels were transferred to the same PVDF membrane so that all gels were processed identically. Total protein isoforms were required to align two-dimensional blots, and thus membranes were incubated with RUBY stain (Bio-Rad) prior to blocking. Protein isoforms stained in this manner were visualized by epi-UV fluorescence, and their locations were marked for alignment purposes. A minimum of 15 reference spots were used to align Tub4p isoforms.

One-Dimensional Electrophoresis, Immunoprecipitation, and Immunoblotting

Extracts were prepared as previously described. SDS-PAGE was performed using a Bio-Rad mini gel apparatus using standard methods. Proteins were separated in 9% gels, transferred to PVDF membranes, and blocked with 2% BSA in TBS/0.1% Tween-20 (TBS/T-20). Membranes were incubated with purified anti-Tub4p antibodies (1:10,000) overnight at 4°C, washed with TBS/T-20, incubated with goat anti-rabbit HRP antibodies (Amersham), washed, and visualized with ECL reagent (Amersham). Anti-Myc antibodies (clone 9E10; Upstate Biotechnology) were used at 1:200 for immunoprecipitations (2 hr at 4°C) and at 1:10,000 for immunoblots. Antigen-IgG complexes were isolated using protein A/G-agarose (Pierce). Anti-Tub2p antibodies (loading control) were used at 1:5000 (Bond et al., 1986).

Acknowledgments

The authors thank Daniel Gelperin, Jessie Hanrahan, Christine Horak, Michael Knop, Michael Smith, and Susana Vidan for comments on the manuscript, and members of the Bloom lab for helpful discussions. This work was supported by the Leslie Warner Cancer fellowship (J.V.) and the National Institutes of Health GM36494 (M.S.).

Received April 12, 2001; revised September 27, 2001.

References

Adames, N.R., and Cooper, J.A. (2000). Microtubule interactions with the cell cortex causing nuclear movements in *Saccharomyces cerevisiae*. J. Cell Biol. *149*, 863–874.

Amon, A., Surana, U., Muroff, I., and Nasmyth, K. (1992). Regulation of p34CDC28 tyrosine phosphorylation is not required for entry into mitosis in *S. cerevisiae*. Nature *355*, 368–371.

Boeke, J.D., LaCroute, F., and Fink, G.R. (1984). A positive selection for mutants lacking orotidine-5′-phosphate decarboxylase activity in yeast: 5-fluoro-orotic acid resistance. Mol. Gen. Genet. *197*, 345–346.

Bond, J., Fridovich-Keil, J., Pillus, L., Mulligan, R., and Solomon, F. (1986). A chicken-yeast chimeric β-tubulin protein is incorporated into mouse microtubules *in vivo*. Cell *44*, 461–468.

Carminati, J.L., and Stearns, T. (1997). Microtubules orient the mitotic spindle in yeast through dynein-dependent interactions with the cell cortex. J. Cell Biol. *138*, 629–641.

Chen, D.C., Yang, B.C., and Kuo, T.T. (1992). One-step transformation of yeast in stationary phase. Curr. Genet. *21*, 83–84.

Geissler, S., Pereira, G., Spang, A., Knop, M., Soues, S., Kilmartin, J., and Schiebel, E. (1996). The spindle pole body component Spc98p interacts with the γ-tubulin-like Tub4p of *Saccharomyces cerevisiae* at the sites of microtubule attachment. EMBO J. *15*, 3899–3911.

Gunawardane, R.N., Martin, O.C., Cao, K., Zhang, L., Dej, K., Iwamatsu, A., and Zheng, Y. (2000). Characterization and reconstitution of *Drosophila* γ-tubulin ring complex subunits. J. Cell Biol. *151*, 1513–1524.

Guthrie, C., and Fink, G.R. (1991). Guide to Yeast Genetics and Molecular Biology (New York: Academic Press).

Horio, T., Uzawa, S., Jung, M.K., Oakley, B.R., Tanaka, K., and Yanagida, M. (1991). The fission yeast γ-tubulin is essential for mitosis and is localized at microtubule organizing centers. J. Cell Sci. *99*, 693–700.

Hoyt, M.A. (2001). Exit from mitosis: spindle pole power. Cell *102*, 267–270.

Jacobs, C.W., Adams, A.E., Szaniszlo, P.J., and Pringle, J.R. (1988). Functions of microtubules in the *Saccharomyces cerevisiae* cell cycle. J. Cell Biol. *107*, 1409–1426.

Keating, T.J., and Borisy, G.G. (2000). Immunostructural evidence for the template mechanism of microtubule nucleation. Nat. Cell Biol. *2*, 352–357.

Kellogg, D., Moritz, M., and Alberts, B. (1994). The centrosome and cellular organization. Annu. Rev. Biochem. *63*, 639–674.

Kilmartin, J.V., and Adams, A.E.M. (1984). Structural rearrangements of tubulin and actin during the cell cycle of the yeast *Saccharomyces*. J. Cell Biol. *98*, 922–933.

Knop, M., and Schiebel, E. (1997). Spc98p and Spc97p of the yeast γ-tubulin complex mediate binding to the spindle pole body via their interaction with Spc110p. EMBO J. *16*, 6985–6995.

Knop, M., and Schiebel, E. (1998). Receptors determine the cellular localization of a γ-tubulin complex and thereby the site of microtubule formation. EMBO J. *17*, 3952–3967.

Knop, M., Pereira, G., Geissler, S., Grein, K., and Schiebel, E. (1997). The spindle pole body component Spc97p interacts with the γ-tubulin of *Saccharomyces cerevisiae* and functions in microtubule organization and spindle pole body duplication. EMBO J. *16*, 1550–1564.

Laemmli, U.K. (1970). Cleavage of structural proteins during the assembly of the head of bacteriophage T4. Nature *227*, 680–685.

Li, R., and Murray, A.W. (1991). Feedback control of mitosis in budding yeast. Cell *66*, 519–531.

Marschall, L., Jeng, R., Mulholland, J., and Stearns, T. (1996). Analysis of Tub4p, a yeast γ-tubulin-like protein: implications for microtubule-organizing center function. J. Cell Biol. *134*, 443–454.

Miller, R.K., and Rose, M.D. (1998). Kar9p is a novel cortical protein required for cytoplasmic or microtubule orientation in yeast. J. Cell Biol. *140*, 377–390.

Minshull, J., Straight, A., Rudner, A.D., Dernburg, A.F., Belmont, A., and Murray, A.W. (1996). Protein phosphatase 2A regulates MPF activity and sister chromatid cohesion in budding yeast. Curr. Biol. *6*, 1609–1620.

Modesti, A., Bini, L., Carraresi, L., Magherini, F., Liberatori, S., Pallini, V., Manao, G., Pinna, L.A., Raugei, G., and Ramponi, G. (2001). Expression of the small tyrosine phosphatase (Stp1) in *Saccharomyces cerevisiae*: a study on protein tyrosine phosphorylation. Electrophoresis *22*, 576–585.

Moritz, M., Braunfeld, M., Fung, J., Sedat, J., Alberts, B., and Agard, D. (1995). Three-dimensional structural characterization of centrosomes from early *Drosophila* embryos. J. Cell Biol. *130*, 1149–1159.

Moritz, M., Braunfeld, M.B., Guenebaut, V., Heuser, J., and Agard, D.A. (2000). Structure of the γ-tubulin ring complex: a template for microtubule nucleation. Nat. Cell Biol. *2*, 365–370.

Murphy, S., Urbani, L., and Stearns, T. (1998). The mammalian γ-tubulin complex contains homologues of the yeast spindle pole body components Spc97p and Spc98p. J. Cell Biol *141*, 663–674.

Nguyen, T., Vinh, D.B., Crawford, D.K., and Davis, T.N. (1998). A genetic analysis of interactions with Spc110p reveals distinct functions of Spc97p and Spc98p, components of the yeast γ-tubulin complex. Mol. Biol. Cell *9*, 2201–2216.

Oakley, C.E., and Oakley, B.R. (1989). Identification of γ-tubulin, a new member of the tubulin superfamily encoded by mipA gene of *Aspergillus nidulans*. Nature. *338*, 662–664.

Oakley, B., Oakley, E., Yoon, Y., and Jung, M.K. (1990). γ-tubulin is a component of the spindle pole body that is essential for microtubule function in *Aspergillus nidulans*. Cell *61*, 1289–1301.

Oegema, K., Wiese, C., Martin, O.C., Milligan, R.A., Iwamatsu, A., Mitchison, T.J., and Zheng, Y. (1999). Characterization of two related *Drosophila* γ-tubulin complexes that differ in their ability to nucleate microtubules. J. Cell Biol. *144*, 721–733.

O'Farrell, P.H. (1975). High resolution two-dimensional electrophoresis of proteins. J. Biol. Chem. *250*, 4007–4021.

Pereira, G., Knop, M., and Schiebel, E. (1998). Spc98p directs the yeast γ-tubulin complex into the nucleus and is subject to cell cycle-dependent phosphorylation on the nuclear side of the spindle pole body. Mol. Biol. Cell *9*, 775–793.

Raff, J.W., Kellogg, D.R., and Alberts, B.M. (1993). *Drosophila* γ-tubulin is part of a complex containing two previously identified centrosomal MAPs. J. Cell Biol. *121*, 823–835.

Rout, M.P., and Kilmartin, J.V. (1990). Components of the yeast spindle and spindle pole body. J. Cell Biol. *111*, 1913–1927.

Sambrook, J., Fritsch, E.F., and Maniatis, T. (1989). Molecular Cloning: A Laboratory Manual, Second Edition (Cold Spring Harbor, NY: Cold Spring Harbor Laboratory Press).

Shaw, S.L., Yeh, E., Maddox, P., Salmon, E.D., and Bloom, K. (1997). Astral microtubule dynamics in yeast: a microtubule-based searching mechanism for spindle orientation and nuclear migration into the bud. J. Cell Biol. *139*, 985–994.

Sikorski, R.S., and Hieter, P. (1989). A system of shuttle vectors and yeast host strains designed for efficient manipulation of DNA in *Saccharomyces cerevisiae*. Genetics *122*, 19–27.

Sobel, S.G., and Snyder, M. (1995). A highly divergent γ-tubulin gene is essential for cell growth and proper microtubule organization in *Saccharomyces cerevisiae*. J. Cell Biol. *131*, 1775–1788.

Sorger, P.K., and Murray, A.W. (1992). S-phase feedback control in budding yeast independent of tyrosine phosphorylation of p34cdc28. Nature *355*, 365–368.

Spang, A., Geissler, S., Grein, K., and Schiebel, E. (1996). γ-Tubulin-like Tub4p of *Saccharomyces cerevisiae* is associated with the spindle pole body substructures that organize microtubules and is required for mitotic spindle formation. J. Cell Biol. *134*, 429–441.

Stearns, T., Evans, L., and Kirschner, M. (1991). γ-tubulin is a highly conserved component of the centrosome. Cell *65*, 825–836.

Straight, A.F., Marshall, W.F., Sedat, J.W., and Murray, A.W. (1997). Mitosis in living budding yeast: anaphase A but no metaphase plate. Science *277*, 574–578.

Tassin, A., Celati, C., Moudjou, M., and Bornens, M. (1998). Characterization of the human homologue of the yeast spc98p and its association with γ-tubulin. J. Cell Biol. *141*, 689–701.

Vogel, J., and Snyder, M. (2000). The carboxy terminus of Tub4p is required for γ-tubulin function in budding yeast. J. Cell Sci. *113*, 3871–3882.

Vogel, J., Stearns, T., Rieder, C., and Palazzo, R. (1997). Centrosomes isolated from *Spisula solidissima* oocytes contain rings and an unusual stoichiometric ratio of α/β tubulin. J. Cell Biol. *137*, 193–202.

Wiese, C., and Zheng, Y. (2000). A new function for the γ-tubulin ring complex as a microtubule minus-end cap. Nat. Cell Biol. *2*, 358–364.

Yeh, E., Yang, C., Chin, E., Maddox, P., Salmon, E.D., Lew, D.J., and Bloom, K. (2000). Dynamic positioning of mitotic spindles in yeast: role of motors and cortical determinants. Mol. Biol. Cell *11*, 3949–3961.

Zhang, L., Keating, T.J., Wilde, A., Borisy, G.G., and Zheng, Y. (2000). The role of Xgrip210 in γ-tubulin ring complex assembly and centrosome recruitment. J. Cell Biol. *151*, 1525–1536.

Zheng, Y., Jung, M.K., and Oakley, B. (1991). γ-tubulin is present in *Drosophila melanogaster* and *Homo sapiens* and is associated with the centrosome. Cell *65*, 817–823.

Zheng, Y., Wong, M.L., Alberts, B., and Mitchison, T. (1995). Nucleation of microtubule assembly by a γ-tubulin-containing ring complex. Nature *378*, 578–583.

Zhu, H., Klemic, J.F., Chang, S., Bertone, P., Casamayor, A., Klemic, K.G., Smith, D., Gerstein, M., Reed, M.A., and Snyder, M. (2000). Analysis of yeast protein kinases using protein chips. Nat. Genet. *26*, 283–289.